Draft version May 24, 2016
Preprint typeset using LaTeX style emulateapj v. 5/2/11

arXiv:1604.08131v2 [astro-ph.HE] 23 May 2016

REVISITING THE CONTRIBUTIONS OF SUPERNOVA AND HYPERNOVA REMNANTS TO THE DIFFUSE HIGH-ENERGY BACKGROUNDS: CONSTRAINTS ON VERY-HIGH-REDSHIFT INJECTION

Di Xiao[1,2,3], Peter Mészáros[3], Kohta Murase[3] and Zi-Gao Dai[1,2]
[1]School of Astronomy and Space Science, Nanjing University, Nanjing 210093, China
[2]Key Laboratory of Modern Astronomy and Astrophysics (Nanjing University), Ministry of Education, China and
[3]Center for Particle and Gravitational Astrophysics; Department of Physics; Department of Astronomy and Astrophysics, The Pennsylvania State University, University Park, PA 16802, USA

(Dated: May 24, 2016)
Draft version May 24, 2016

ABSTRACT

Star-forming and starburst galaxies are considered as one of the viable candidate sources of the high-energy cosmic neutrino background detected in IceCube. We revisit contributions of supernova remnants (SNRs) and hypernova remnants (HNRs) in such galaxies to the diffuse high-energy neutrino and gamma-ray backgrounds, in light of the latest *Fermi* data above 50 GeV. We also take into account possible time dependent effects of the cosmic-ray (CR) acceleration during the SNR evolution. CRs accelerated by the SNR shocks can produce high-energy neutrinos up to ~ 100 TeV energies, but CRs from HNRs can extend the spectrum up to PeV energies. We show that, only if HNRs are dominant over SNRs, the diffuse neutrino background above 100 TeV can be explained without contradicting the gamma-ray data. However, the neutrino data around 30 TeV remain unexplained, which might suggest a different population of gamma-ray dark CR sources. We also consider possible contributions of Pop-III HNRs up to $z \lesssim 10$, and show that they are not constrained by the gamma-ray data, and thus could contribute to the diffuse high-energy backgrounds if their explosion energy reaches $\mathcal{E}_{\rm POP-III} \sim$ a few $\times 10^{53}$ erg. More conservatively, our results suggest that the explosion energy of POP-III HNRs is $\mathcal{E}_{\rm POP-III} \lesssim 7 \times 10^{53}$ erg.

Subject headings: supernova remnants, neutrinos, diffuse gamma-rays

1. INTRODUCTION

During last few years the IceCube experiment has detected tens of high-energy astrophysical neutrinos from 10 TeV to a few PeV (Aartsen et al. 2013a,b, 2015). This outstanding observation result has led to a wide debate about the origin of these neutrinos, (e.g., Mészáros 2014; Murase 2015). Among various source models, the most commonly discussed are SNRs (like W49B (Lopez et al. 2013; González-Casanova et al. 2014)) in star-forming galaxies (SFGs) and starbursts galaxies (SBGs) (e.g., Loeb & Waxman 2006; Murase et al. 2013; Liu et al. 2014; Tamborra et al. 2014; Anchordoqui et al. 2014; Chang & Wang 2014, 2015; Senno et al. 2015), which are good cosmic-ray (CR) reservoirs and can produce neutrinos via *pp* interactions. At the same time, this interaction will produce a certain amount of gamma-rays and contribute to the extragalactic gamma-ray background (EGB), and a common origin of the diffuse backgrounds has been suggested (Murase et al. 2013). Other possible astrophysical sources which can contribute to the IceCube neutrino flux include gamma-ray bursts (GRBs) (Waxman & Bahcall 1997; Mészáros & Waxman 2001; Murase 2008; Wang & Dai 2009; Bustamante et al. 2015; Xiao & Dai 2014, 2015; Tamborra & Ando 2016), low-luminosity GRBs or trans-relativistic supernovae (SNe) (Murase et al. 2006; Gupta & Zhang 2007; Murase & Ioka 2013; Senno et al. 2016), active galactic nuclei (Stecker et al. 1991; Alvarez-Muñiz & Mészáros 2004; Anchordoqui et al. 2008; Stecker 2013; Murase et al. 2014; Dermer et al. 2014; Petropoulou et al. 2015), galaxy clusters and groups (Murase et al. 2008), newborn pulsars (Murase et al. 2009; Fang et al. 2014). Alternatively, there are also arguments about a possible Galactic contribution (e.g., Fox et al. 2013; Ahlers & Murase 2014; Taylor et al. 2014; Neronov & Semikoz 2016).

On the other hand, the Fermi-LAT instrument has measured the EGB in the energy range from 0.1 to 820 GeV (Ackermann et al. 2015). New studies of the blazar flux distribution at gamma-ray energies above 50 GeV have shown that most of the EGB flux should be contributed by blazars, at a percentage level $86^{+16}_{-14}\%$ (Bechtol et al. 2015; Fermi Collaboration 2016). This means that the diffuse gamma-ray flux from other sources cannot exceed the residual non-blazar component, which puts a strong constraint on the SBG scenario (Murase et al. 2013). Murase et al. (2016) found that SBGs cannot explain the IceCube data below 100 TeV especially if the above constraint on the non-blazar component is taken into account. More quantitatively, Bechtol et al. (2015) argued, from the known branching ratio between charged and neutral pion production, that the gamma-ray emission of SBGs explaining the IceCube data would be well beyond 14%, so these observational results would be in strong tension with the SBG scenario. Interestingly, similar results are also found by the gamma-ray anisotropy data (Ando et al. 2015).

In this work, we argue that if we attribute, as is common, the production of CRs in SBGs to SNRs, then taking into account the time-behavior of the SNR evolution, and taking into account also a contribution from very-high-redshift SNRs in a Pop-III component, it is possible to reduce the portion of the EGB which is in tension with Fermi, so that SBGs could contribute a potentially

interesting fraction of the IceCube neutrino flux.

We assume that the neutrinos are mainly produced at the end of the free expansion and during the Sedov-Taylor phase of the SNR, in which the maximum CR energy and maximum neutrino energy naturally decreases with time due to a decreasing expansion velocity and magnetic field in the shock. For the accompanying γ-rays, after the $\gamma\gamma$ cascade process, this also translates into a different "elbow" of the EGB.

The total CR energy injection rate during the evolution may be uncertain, and here we parametrize it as a simple universal power law in time during the Sedov phase, $L_{\rm CR} \propto t^{\alpha}$, with α ranging from zero to negative values. We then discuss the impact of α on the final neutrino and gamma-ray spectrum. We found that negative values of α are more favorable from the point of view of attributing a significant fraction of the neutrino and gamma-ray background to SNRs, including both normal HNe and SNe, as discussed below. Conversely, an appreciable contribution of SBG SNRs to these backgrounds would have implications for the acceptable values of α, and thus for the CR production efficiency as a function of the SNR dynamics.

One main difference between our paper and previous work is that we allow for a wider range of HN ejecta energies, and we allow for the different CR maximum energy and flux contribution at different stages of the SNR expansion. The other, more significant major difference is that we allow for a Pop-III population of SNRs, with a comparable cosmic ray acceleration efficiency and comparable or larger kinetic energy as those attributed to $z \lesssim 4$ SNRs and HNRs.

This paper is organized as follows. We introduce the model and method of calculation in Section 2. Then section 3 presents our results showing the combined fits of our model compared with the IceCube and Fermi EGB data. The implications of the results are presented in Section 4.

2. MODEL AND METHOD OF CALCULATION

2.1. *Sedov-Taylor Phase of Supernova Remnant*

After the early free expansion, the evolution of a SNR enters the Sedov-Taylor self-similar expansion phase (Sedov 1959; Taylor 1950). The ejected remnant shell collides with and sweeps up the ambient medium, forming a shock which can accelerate CRs that subsequently, via *pp* collisions, produce high energy neutrinos and γ-rays. We take the beginning of the Sedov-Taylor phase as the onset time for CR acceleration and secondary neutrino and γ-ray production. This occurs at a time

$$t_0 = \frac{R_{\rm dec}}{v_{\rm ej}} = \frac{(3M_{\rm ej}/4\pi m_p n_0)^{1/3}}{(2\mathcal{E}_{\rm SN}/M_{\rm ej})^{1/2}} \simeq 1.4\times10^3 \mathcal{E}_{\rm SN,51}^{-1/2} n_{0,0}^{-1/3} M_{\rm ej,1}^{5/6}\,{\rm yr} \quad (1)$$

after the initial explosion. The ending time of the Sedov-Taylor phase $t_{\rm end}$ occurs when the adiabatic expansion approximation is no longer true, and this is determined by equating the cooling time of the post-shock region with the SNR dynamic time. The gas cooling function has been evaluated in detail by (e.g. Sutherland & Dopita 1993), and has been adopted in our calculation to solve for $t_{\rm end}$ as a function of different sets of parameters.

We take the usual time dependence of the radius and the shock velocity in the Sedov-Taylor phase $R = (25\mathcal{E}_{\rm SN}/4\pi m_p n_0)^{1/5} t^{2/5}$ and $v = (2/5)(25\mathcal{E}_{\rm SN}/4\pi m_p n_0)^{1/5} t^{-3/5}$ (Sedov 1959; Taylor 1950; Ramirez-Ruiz & MacFadyen 2010), and the commonly used estimate for the post-shock magnetic field $B = (9\pi\epsilon_B m_p n_0 v^2)^{1/2}$ where $\epsilon_B \leq 1$ is the ratio of the post-shock magnetic to thermal energy. In this work, we will assume the CR component to be pure protons. Then, for diffusive shock acceleration, the maximum proton energy is estimated by equating the local acceleration time to the dynamical time (the cooling timescale for *pp* collisions and synchrotron losses being much longer than the dynamical timescale, e.g. Senno et al. (2015)), which gives $(20\epsilon_{p,\rm max}c/3eB) = Rv$ (Drury 2011). Thus, in the Sedov-Taylor phase the maximum CR energy also depends on time,

$$\epsilon_{p,\rm max} = 1.58\times10^6 \mathcal{E}_{\rm SN,51} n_{0,0}^{1/6} M_{\rm ej,1}^{-2/3} \epsilon_{B,-2}^{1/2} (t/t_0)^{-4/5}\ {\rm GeV} \quad (2)$$

2.2. *Energy injection into CRs*

In the free expansion phase, for an external density $\rho =$ constant, as long as the swept-up mass is small the velocity $v \simeq$ constant and the radius grows as $R \propto t$. The rate at which mass is swept and is shock-heated is $\dot{M} \propto R^2\rho v \propto R^2 \propto t^2$, and the bolometric luminosity that can go into CRs grows as $L \propto \dot{M} \propto t^2$. The equipartition post-shock field behaves as $B \propto v \propto$ constant, and the shock strength is also constant. Thus, at the simplest level one expects the CR bolometric luminosity to grow as $L_{\rm CR} \propto t^2$. In the Sedov phase, on the other hand, $R \propto t^{2/5}$ and $v \propto t^{-3/5}$ so one expects $\dot{M} \propto t^{1/5}$, while $B \propto v \propto t^{-3/5}$, and with decreasing velocity the shock strength decreases. Thus, one does not expect a positive proportionality between $\dot{M}$ and $L_{\rm CR}$ but instead a decrease of $L_{\rm CR}$ can be expected. The SN ejecta begins to slow down at t_0 when it has swept up an amount of external mass comparable to that of the ejecta shell, marking the beginning of the Sedov-Taylor phase, when the cosmic ray acceleration is expected to peak. The details of the continued CR injection as the blast wave slows down in the Sedov-Taylor phase are model-dependent, and here we shall parametrize it as

$$L_{\rm CR}(t) = \mathcal{A}(t/t_0)^{\alpha}, \quad (3)$$

where $\mathcal{A}$ is a normalization factor determined by $\int_{t_0}^{t_{\rm end}} L_{\rm CR} dt = \eta\mathcal{E}_{\rm SN}$. Here $\eta \sim 0.1$ is the CR acceleration efficiency (Caprioli et al. 2015). According to equation (3), at different stages of the Sedov-Taylor phase, the energy injection rate into CRs will be different. The value $\alpha = -1$ is a nominal steady injection case (Ohira et al. 2010). Because of the very fast growth $L_{\rm CR} \propto t^2$ in the initial free expansion phase, for simplicity we neglect contributions from this phase. We shall assume the shock-accelerated proton spectrum to be a power law $dN_p/d\epsilon_p \propto \epsilon_p^{-p}$ with index $p = 2$, so at time t, the proton spectrum being written as:

$$\epsilon_p L_{\epsilon_p}(t) = \begin{cases} \frac{L_{\rm CR}(t)}{\mathcal{C}} & \text{if } \epsilon_p \leq \epsilon_{p,\rm max}(t) \\ \frac{L_{\rm CR}(t)}{\mathcal{C}} e^{-\epsilon_p/\epsilon_{p,\rm max}} & \text{if } \epsilon_p > \epsilon_{p,\rm max}(t) \end{cases} \quad (4)$$

where $\mathcal{C} = \ln(\epsilon_{p,\max}/\epsilon_{p,\min})$

2.3. *Diffuse Neutrino and Gamma-ray Fluxes*

Hypernovae (HNe) are a sub-type of supernovae (SNe) which are more energetic but relatively rarer. Recent studies indicate that the total rate of all core-collapse supernovae (CCSNe) is $\mathcal{R}_{\rm CCSNe} = (1.06\pm0.11(stat)\pm0.15(sys))\times10^{-4}(h_0/0.7)^3{\rm Mpc}^{-3}{\rm yr}^{-1}$ (Taylor et al. 2014). For typical HNe, the kinetic energy is of order 10^{52-53}erg, with a typical rate $\mathcal{R}_{\rm HNe} \leq 4\%\mathcal{R}_{\rm CCSNe}$ (Guetta & Della Valle 2007; Arcavi et al. 2010; Senno et al. 2015), but with substantial uncertainties. HNe have been discussed as possible sources for high-energy cosmic rays (Dermer 2002; Sveshnikova 2003; Wang et al. 2007; Ioka & Mészáros 2010). Due to larger kinetic energy, HNe can lead to larger maximum proton energies and will dominate the neutrino flux at PeV energies.

The total local CR energy budget is

$$\epsilon_p Q_{\epsilon_p}(z=0) = \mathcal{R}_{\rm SNe}\int_{t_{0,\rm SNe}}^{t_{\rm end,SNe}} \epsilon_p L_{\epsilon_p}^{\rm SNe}(t)dt + \mathcal{R}_{\rm HNe}\int_{t_{0,\rm HNe}}^{t_{\rm end,HNe}} \epsilon_p L_{\epsilon_p}^{\rm HNe}(t)dt \quad (5)$$

and the cosmological evolution of sources can be expressed as $\epsilon_p Q_{\epsilon_p}(z) = \epsilon_p Q_{\epsilon_p}(z=0)S(z)$, in which the evolution term is $S(z) = [(1+z)^{-34} + (\frac{1+z}{5000})^3 + (\frac{1+z}{9})^{35}]^{-0.1}$ (Hopkins & Beacom 2006; Yüksel et al. 2008). In this work, the typical neutrino energy is approximated to be $E_\nu \sim 0.05\epsilon_p/(1+z)$.

The diffuse neutrino flux per flavor is calculated as (e.g., Murase et al. 2013; Senno et al. 2015; Bechtol et al. 2015; Murase et al. 2016)

$$E_\nu^2\Phi_{\nu_i} = \frac{c}{4\pi H_0}\int_0^{z_{\max}} \frac{\min[1,f_{pp}]}{6} \times \frac{\epsilon_p Q_{\epsilon_p}(z=0)S(z)}{(1+z)^2\sqrt{\Omega_M(1+z)^3+\Omega_\Lambda}}dz \quad (6)$$

where $z_{\max}=4$, the cosmology parameters are $H_0 = 67.8\,{\rm km\,s^{-1}\,Mpc^{-1}}, \Omega_M = 0.308$ (Plank Collaboration 2015) and $f_{pp} = \bar{n}\kappa\sigma_{pp}c\cdot\min[t_{\rm diff}, t_{\rm adv}]$. Here the diffusive escape timescale of CRs from the host galaxy is $t_{\rm diff} = h^2/4D$, where h is the galaxy scale-height, the diffusion coefficient is $D(\epsilon_p) = D_c[(\epsilon_p/\epsilon_{p,c})^{1/3} + (\epsilon_p/\epsilon_{p,c})^2]$ and the timescale of advective escape is $t_{\rm adv} = h/V_w$. We use the values of $h = 10^{21}$cm, $D_c \sim 3.1\times10^{29}{\rm cm^2\,s^{-1}}$, $\epsilon_{p,c}\sim 9.3\times10^9$GeV, $V_w = 1500{\rm km\,s^{-1}}$, $B = 4$mG, $\bar{n} = 100{\rm cm^{-3}}$ for SBGs (Strickland & Heckman 2009) and $h = 1$kpc, $D_c\sim 3.1\times10^{29}{\rm cm^2\,s^{-1}}$, $\epsilon_{p,c}\sim 9.3\times10^6$GeV, $V_w = 500{\rm km\,s^{-1}}$, $B = 1\mu$G, $\bar{n} = 1{\rm cm^{-3}}$ for SFGs (Keeney et al. 2006; Crocker 2012). We assume a starburst fraction of $\xi_{\rm SBG} = 0.1$ (Tamborra et al. 2014). Note that the upstream magnetic field of SBGs can be stronger than in the usual ISM due to the superbubble structure. Also, the upstream field amplification by CRs may be expected (Beresnyak et al. 2009). A further contribution to f_{pp} from diffusion in the host galaxy cluster is considered in Senno et al. (2015).

Based on the standard branching ratio between charged and neutral pion production of *pp* interaction, the gamma-ray flux can initially be related to the neutrino flux through $E_\gamma^2\Phi_\gamma = 2E_\nu^2\Phi_\nu|_{\epsilon_\nu=0.5\epsilon_\gamma}$. However, once they are produced, high energy gamma-rays undergo $\gamma\gamma$ interactions. The main target soft photons are from the extragalactic background light (EBL) (e.g., Salamon & Stecker 1998; Dai & Lu 2002; Dai et al. 2002; Murase et al. 2012). The optical depth for gamma-rays depends on their energy ϵ_γ, as well as on redshift, because the EBL intensity varies at different z (Finke et al. 2010). We can set $\tau_{\gamma\gamma}(E_\gamma, z) = 1$ to get the cut-off energy $E_\gamma^{\rm cut}$. Beyond $E_\gamma^{\rm cut}$, electromagnetic cascade develops, and the resulting spectrum has a universal form (Berezinskii & Smirnov 1975; Murase et al. 2012),

$$E_\gamma\frac{dN_\gamma}{dE_\gamma} \propto \begin{cases} (\frac{E_\gamma}{E_\gamma^{\rm br}})^{-1/2} & \text{if } E_\gamma \leq E_\gamma^{\rm br} \\ (\frac{E_\gamma}{E_\gamma^{\rm br}})^{-1} & \text{if } E_\gamma^{\rm br} < E_\gamma \leq E_\gamma^{\rm cut} \end{cases} \quad (7)$$

where $E_\gamma^{\rm br} = 0.0085(1+z)^2(\frac{E_\gamma^{\rm cut}}{100{\rm GeV}})^2$ (Senno et al. 2015). The normalization is determined by integrating the gamma-ray flux over $E_\gamma^{\rm cut}$.

Below $E_\gamma^{\rm cut}$, the gamma-ray intensity is attenuated by a factor $e^{-\tau_{\gamma\gamma}}$. This is calculated similarly to the diffuse neutrino flux, with a typical energy $E_\gamma \sim 0.1\epsilon_p/(1+z)$,

$$E_\gamma^2\Phi_\gamma = \frac{c}{4\pi H_0}\int_0^{z_{\max}} \frac{\min[1,f_{pp}]}{3} \times \frac{\epsilon_p Q_{\epsilon_p}(z=0)S(z)}{(1+z)^2\sqrt{\Omega_M(1+z)^3+\Omega_\Lambda}}e^{-\tau_{\gamma\gamma}(E_\gamma,z)}dz \quad (8)$$

The final diffuse gamma-ray flux is the sum of these two components.

3. RESULTS

3.1. *The $z \lesssim 4$ contribution*

Here we use the above discussed values of the luminosity functions, the EBL density and other parameters which are commonly used for redshifts $z \lesssim 4$. Figure 1 shows a combined fit of the diffuse gamma-ray and neutrino flux for the nominal case of $\alpha = -1$ in eq. (3). We use this nominal value to delimit the physically expected range of $\alpha \lesssim 0.5$. The IceCube neutrino and Fermi-LAT extragalactic gamma-ray background (EGB) observation are shown by the blue and red data points respectively. The black solid line is the predicted total diffuse neutrino flux and the red solid line represents the gamma-ray flux. The black dashed and dotted line represent the contribution to the neutrino flux from SNe and HNe respectively. We can see that HNe dominate the PeV neutrino flux, while SNe only contribute up to sub-PeV neutrino energies. However, this case based on the conventional assumptions cannot explain the IceCube data, suggesting that the HN rate would need to be enhanced to explain the neutrino data. This difficulty in getting a good combined ν,γ fit for this conventional case is compatible with the independent generic arguments of Bechtol et al. (2015) against SBGs being the dominant sources of IceCube neutrinos.

Obviously, we would expect to increase the fraction of HNe contribution because they can achieve higher CR energies. Figure 2 shows what happens if we increase the HNe kinetic energy to $10^{52.5}$erg. The blue solid line

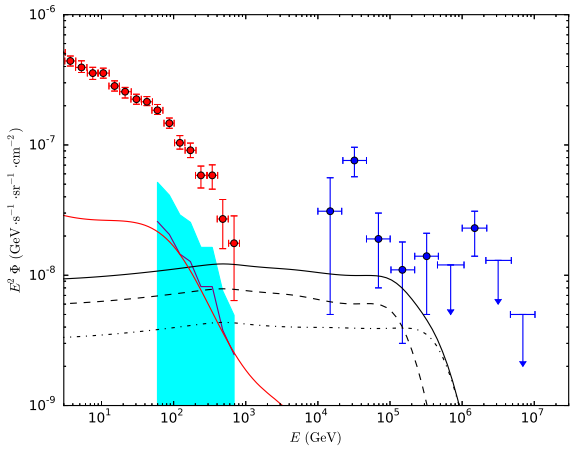

FIG. 1.— Combined fit of diffuse neutrino flux and gamma-ray flux for the case $\alpha = -1$ for the conventional case. The IceCube neutrino and the Fermi-LAT extragalactic gamma-ray background observations are shown by blue and red data points respectively (Ackermann et al. 2015; Aartsen et al. 2015). The cyan area shows the allowed region for the non-blazar gamma-ray flux in Fermi Collaboration (2016) and the best-fit 14% residual of the Fermi EGB is marked by the purple solid line. Black dashed and dotted lines represent the calculated contribution to the neutrino flux from SNe and HNe respectively, from the range $z \leq 4$. The black solid line is the predicted total diffuse neutrino flux and the red solid line is the predicted gamma-ray flux. The main parameters are $\mathcal{E}_{\rm SNe} = 5 \times 10^{50}$erg, $\mathcal{E}_{\rm HNe} = 10^{52}$erg, $\eta = 0.1$, $n_0 = 1{\rm cm}^{-3}$,$\mathcal{R}_{\rm HNe} = 3\%\mathcal{R}_{\rm CCSNe}$. The SBG magnetic field is set to $B = 1$ mG.

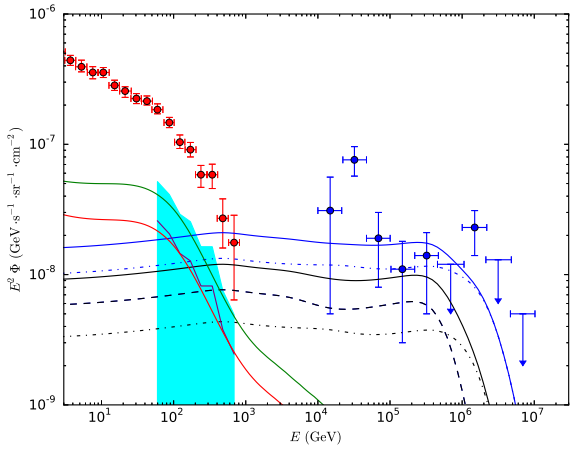

FIG. 2.— The same as Figure 1 but with $\mathcal{E}_{\rm HNe} = 10^{52.5}$erg. The blue solid line is the total neutrino flux, which is the sum of SNe (blue dashed line) and HNe (blue dotted line) contributions. The green solid line is the diffuse gamma-ray flux in this case. The SBG magnetic field is set to $B = 4$ mG. Black lines show the neutrino spectrum for a $\mathcal{E}_{\rm HNe} = 10^{52}$erg case for comparison (SNe-black dashed, HNe-black dotted, total-black solid), while the red solid line is the corresponding diffuse gamma-ray flux.

is the diffuse neutrino flux, which satisfies the observations better now, although it is still below the 1σ range of the last data point. The SN contribution is the blue dashed line and the HN are the blue dotted line. Except for $\mathcal{E}_{\rm HNe}$, all other parameters are the same for the black lines in this figure. The corresponding gamma-ray flux is the green solid line, which is still in the allowed range. In this case, the ratio between the HNe and SNe contribution is $\zeta \equiv \frac{\eta\mathcal{E}_{\rm HN}\mathcal{R}_{\rm HN}}{\eta\mathcal{E}_{\rm SN}\mathcal{R}_{\rm SN}} = \frac{10^{52.5}\times 3\%}{5\times 10^{50}\times 97\%} \sim 2$, compared to $\zeta \sim 0.6$ for the $\mathcal{E}_{\rm HN} = 10^{52}$erg case. We can draw a rough conclusion that $\zeta \gtrsim 1$ is needed for a good fit.

In addition, we consider more realistic cases where $L_{\rm CR} \propto t^{\alpha}$, for various α. We plot the combined fits for different values of α in Figure 3. The neutrino spectrum shape is seen to depend on α. Looking at the results for $\alpha = 0$ and for positive values $\alpha = 1, 2$ (although the positive values are unlikely to occur) we see that all three neutrino spectral curves decrease sharply at the high energy end, undershooting the data. One way to address this might be to increase the rate of HNe (or to choose a very large SBG fraction $\xi_{\rm SBG}$), thus increasing the energy input of HNe so as to reach the IceCube data, but this inevitably gives rise to an increased gamma-ray flux which would overshoot the Fermi data. However, for the physically more reasonable negative α values, the neutrino spectrum is "flatter" (since at later times in the HN evolution both the maximum energy and the flux decrease) and more energy is evident in the flux at the high energy end, so we do not need such a high fraction of HNe as before. We can see that the last IceCube data point is reachable for $\alpha = -2$ and $\alpha = -3$ using a quite conservative HN fraction $\mathcal{R}_{\rm HNe} = 3\%\mathcal{R}_{\rm CCSNe}$. Clearly, negative values of α are more favorable from an observational point of view.

Generally, the parameter space gets larger for smaller α. The major parameters that we can adjust in our fits include the SBG upstream magnetic field; the kinetic energies $\mathcal{E}_{\rm SN}$, $\mathcal{E}_{\rm HN}$; the pre-shock medium number density n_0; the HNe fraction $\mathcal{R}_{\rm HN}$; and the CR acceleration efficiency η. The nominal values used here are in the observationally reasonable range, e.g. $B = 4$mG (e.g. Thompson et al. 2006; Robishaw et al. 2008; Beck 2016), $\mathcal{E}_{\rm SN} \sim 10^{50-51}{\rm erg}, \mathcal{E}_{\rm HN} \sim 10^{52-53}$erg (e.g. Iwamoto et al. 1998; Mazzali et al. 2003), $n_0 \sim 1$ cm^{-3} (Draine & Woods 1991; Chevalier & Claes 2001; Koo et al. 2007; Fox et al. 2011), $\mathcal{R}_{\rm HNe} \leq 0.04\mathcal{R}_{\rm CCSNe}$ (Guetta & Della Valle 2007; Arcavi et al. 2010) and $\eta < 1$ (physically required). For illustration, Figure 4 shows what happens if we change the SBG upstream magnetic field. A stronger field helps to explain the observations. The key issue here is that we wish to achieve higher maximum proton energies in order to account for PeV neutrino flux.

Alternatively, given the contribution of other sources such as blazars to the Fermi gamma-ray background (Bechtol et al. 2015; Fermi Collaboration 2016), we can provide limits on the SNR contributions to the neutrino flux. If we normalize the gamma-ray flux to the best-fit 14% of the total EGB, we find that for our nominal parameters the corresponding diffuse neutrino flux is about 50% of the observed value, provided that we choose not to satisfy the ~ 30 TeV neutrino data point, which however has small error bars. If this data point has a different physical origin than the higher energy data points, SBGs may still contribute a potentially interesting fraction of the $\gtrsim 100$ TeV IceCube neutrino flux.

One may wonder whether very-high-energy gamma-rays may be attenuated inside SFGs and SBGs. This could happen above $\sim$ 10 TeV energies (Lacki & Thompson 2013; Murase et al. 2013; Chang & Wang 2014). However, this would not change

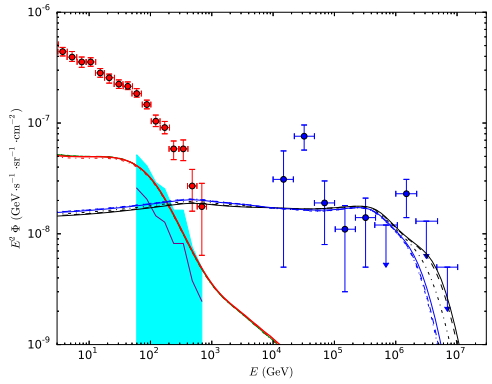

FIG. 3.— Combined fits of diffuse neutrino flux and gamma-ray flux for $z \leq 4$ and different values of the SNR evolution parameter α of equation (3). The IceCube and Fermi-LAT EGB observations are shown by blue and red data points respectively. All parameters are the same as in Figure 2, with predicted neutrino fluxes and gamma-ray fluxes shown by different sets of lines for different α. The values for $\alpha = -3$ are the black solid line and red solid line; $\alpha = -2$ are the black dashed line and red dashed line; $\alpha = -1$ are black dotted line and red dotted line; $\alpha = 0$ are blue solid line and green solid line. For completeness, we also show cases for positive α: $\alpha = 1$ are blue dashed line and green dashed line; $\alpha = 2$ are blue dotted line and green dotted line.

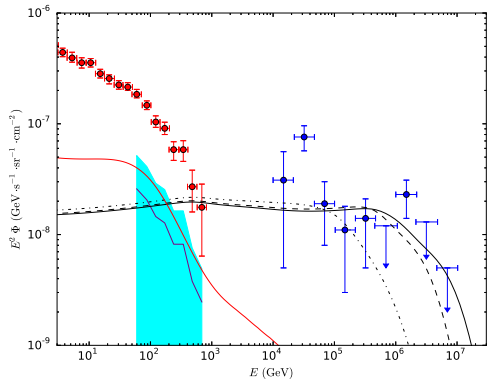

FIG. 4.— The dependence of neutrino flux on the SBG upstream magnetic field, for $z \leq 4$. We choose the $\alpha = -1$ case as an example. The dashed line is for $B = 4$mG, while the solid line is for $B = 10$mG (optimistic) and the dotted line is for $B = 1$mG.

the results essentially. The synchrotron losses of the cascade electron-positron pairs leads to a reduction in the diffuse gamma-ray flux. However, gamma-rays in the 0.1-10 TeV range remain unattenuated in the sources and will be injected into intergalactic cascades. Also, electron-positron pairs including the contribution from muon decays as well as primary electrons produce some gamma-rays, which can make the constraints tighter (Lacki et al. 2014).

3.2. *A possible Pop-III contribution at* $4 \lesssim z \lesssim 10$

An interesting but more uncertain contribution to the diffuse neutrino and gamma-ray background can be expected from the Pop-III star formation occurring at high redshifts (e.g. Umeda & Nomoto 2003; Iwamoto et al. 2005). For these epochs, besides the increased redshift of the received photons, also (other things being equal) the $(1+z)^3$ increase of the proper densities affects the $\gamma\gamma$ interaction and the gamma-ray attenuation. Pop-III stars are extremely metal-poor and can be very massive (e.g. Abel et al. 2002; Hosokawa et al. 2011; Whalen et al. 2013; Yang et al. 2015). They may end their life as HN explosions, $\mathcal{E}_{\rm kin} = 10^{51-53}$erg (e.g. Chen 2014; Tominaga et al. 2014; Toma et al. 2016), and such Pop-III SNe, including jet-driven SNe and GRBs, are also expected to accelerate CRs and produce neutrinos (Schneider et al. 2002; Iocco et al. 2008; Gao et al. 2011; Berezinsky & Blasi 2012).

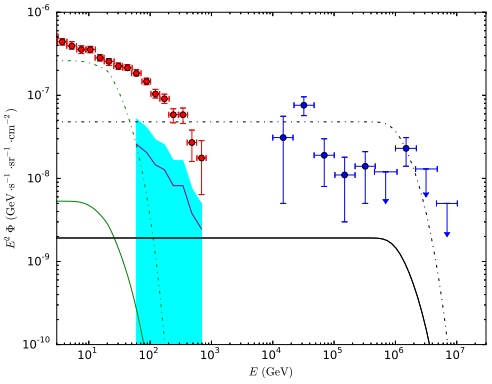

FIG. 5.— Possible contribution from Pop-III HNRs with $4 \leq z \leq 10$ by themselves. Black and green lines represent the predicted diffuse neutrino and gamma-ray fluxes respectively. For the solid lines the efficiency η is 0.1 and the kinetic energy is $\mathcal{E}_{\rm kin} = 10^{52.5}$ erg. For the dotted-dashed lines, the value of $\eta\mathcal{E}_{\rm kin}$ (i.e. the flux) is multiplied by a factor 25. These dotted-dashed lines serve as an upper bound for the Pop-III contribution.

The theoretical uncertainties for this Pop-III epoch are significant, but we can use assume reasonable HN parameters used in the literature for illustrative purposes. For instance, the Pop-III star formation rate is under debate (Wise & Abel 2005; Bromm & Loeb 2006; Trenti & Stiavelli 2009; de Souza et al. 2011; Wise et al. 2012) and can be $10-100$ times smaller (Trenti & Stiavelli 2009; Wise et al. 2012). Here, we use the HN explosion parameters of Chen (2014); Tominaga et al. (2014) and the EBL model and the upper Pop-III model given in Inoue et al. (2013), with a typical HN kinetic energy of $\mathcal{E}_{\rm kin} = 10^{52.5}$ erg and an external gas density $n_0 = 10^3$ cm^{-3}, the latter value being compatible with gas densities inferred from the $z \sim 6.3$ GRB afterglow analysis of Gou et al. (2007). Neglecting at first entirely the contribution of SNe and HNe at $z \leq 4$, we plot in Figure 5 the contribution of only these Pop-III HNe to the neutrino and gamma-ray flux received form the redshift range $4 \leq z \leq 10$, using the $\alpha = -1$ case as an example.

From this figure 5 it is seen that such Pop-III HNe would likely make only a minor contribution to the diffuse neutrino flux. However, if the explosion energy is larger, $\mathcal{E}_{\rm POP-III} \sim 10^{53}$ erg, these POP-III HNe by themselves may be able to fit the neutrino data well, without violating the Fermi-LAT 14% residual background. Actually, there is still a larger parameter space for this fitting, as evidenced by the upper bound shown in Figure 5, making Pop-III stars more interesting sources for the present purposes. Alternatively, our results suggest that their explosion energy is limited to $\mathcal{E}_{\rm POP-III} \lesssim 7 \times 10^{53}$ erg.

Based on this Pop-III model, we also explore the in-

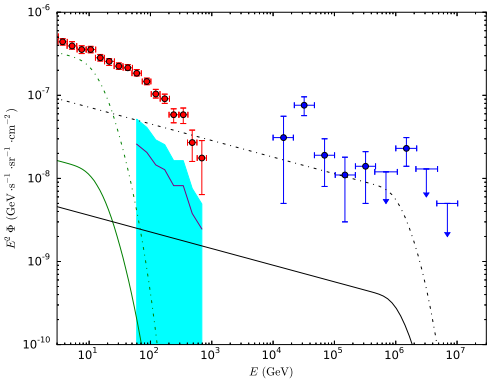

FIG. 6.— Same as Figure 5 but with a CR spectrum index $p = 2.2$. For the solid lines the efficiency $\eta = 0.1$ and $\mathcal{E}_{\rm kin} = 10^{52.5}$ erg, while for the dotted-dashed lines, $\eta\mathcal{E}_{\rm kin}$ (i.e. the flux) is multiplied by a factor 20.

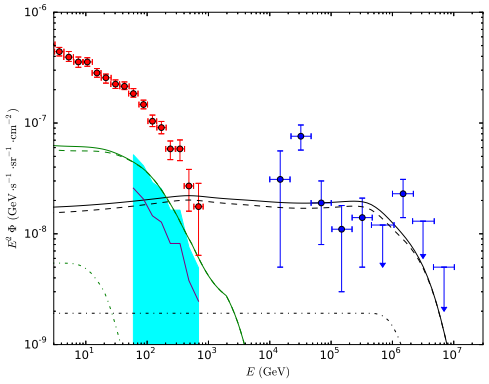

FIG. 7.— An example for two component (low and high redshift) contribution. Black and green solid lines represent the total diffuse neutrino flux and gamma-ray flux, while the dashed lines are the $z \leq 4$ SNe/HNe and the dotted lines are the Pop. III SNe. The CR contribution of the Pop. III is instrumental in making this fit more complete and reasonable, with a fiducial CR efficiency $\eta = 0.1$ for both populations.

fluence that the initial CR spectral index p has on the results. Figure 6 shows the case $p = 2.2$. Solid lines are for $\eta = 0.1$ and dashed lines are for an enhancement by a factor of 20, while other parameters remain unchanged from Figure 5. We see that at high energies the upper bound is lower than that of the $p = 2$ case. This means that for $p = 2.2$, under the same constraint given by Fermi-LAT, less neutrino flux can be attributed to the Pop-III stars. From this point of view, the smaller p are more favorable. We can give a rough constraint of $p \leq 2.2$.

Of course there is no reason to assume that only Pop-III HNRs contribute neutrinos in the IceCube energy range, so a more realistic scenario would involve at least two components contributing to the neutrino flux, one being the standard SNe and HNe in the usual redshift range $z \leq 4$, and the other being the Pop-III HNe in the $4 \leq z \leq 10$ range. The occurrence rates in the lower redshift range are observationally better constrained than for the Pop-III component, but the ratio between the two has large uncertainties. Since $E_\nu^2\Phi_{\nu_i} \propto \eta\mathcal{E}\mathcal{R}$, the ratio between the Pop-III and Pop-I/II CR contribution can be written as

$$\frac{(E_\nu^2\Phi_{\nu_i})_{\rm III}}{(E_\nu^2\Phi_{\nu_i})_{\rm I/II}} = \frac{\eta\mathcal{E}_{\rm HN}\mathcal{R}_{\rm III}(\bar{z}_{\rm III})}{\eta\mathcal{E}_{\rm SN}0.97\mathcal{R}_{\rm I/II}(\bar{z}_{\rm I/II}) + \eta\mathcal{E}_{\rm HN}0.03\mathcal{R}_{\rm I/II}(\bar{z}_{\rm I/II})} \times \frac{(1+\bar{z}_{\rm I/II})^2\sqrt{\Omega_M(1+\bar{z}_{\rm I/II})^3+\Omega_\Lambda}}{(1+\bar{z}_{\rm III})^2\sqrt{\Omega_M(1+\bar{z}_{\rm III})^3+\Omega_\Lambda}}\frac{f_{pp}^{\rm III}}{f_{pp}^{\rm I/II}}. \quad (9)$$

Here, as seen also from Fig. 8, the first term is ~ 0.3, where the typical redshifts of POP I/II and POP III remnants are $\bar{z}_{\rm I/II} \sim 1$ and $\bar{z}_{\rm III} \sim 5$, respectively. The second term gives ~ 0.02 and the last term is ~ 20, leading to the ratio is ~ 0.1. The star formation rate will be lower for Pop-III than it is at low redshifts. On the other hand, $\eta\mathcal{E}\mathcal{R}(z)$ could be substantially larger due to a plausibly larger kinetic energy. Thus, introducing this Pop-III contribution potentially allows one to produce a fraction approaching unity of the low and high redshift IceCube neutrino flux, without violating the Fermi residual gamma-ray background. An example with these two components is shown in Figure 7, where the Pop-III/Pop-I/II efficiency is set to the same $\eta = 0.1$. We can see that Pop-III HNe can contribute an interesting fraction to the diffuse neutrino flux, providing a good argument in favor of SBG scenario.

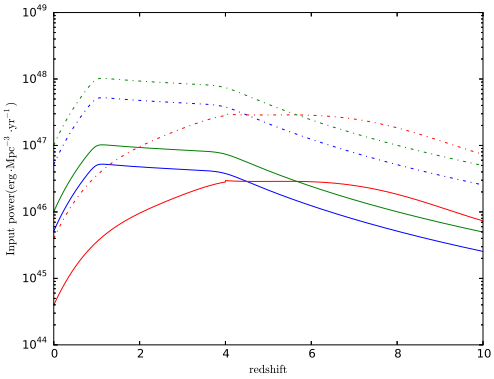

FIG. 8.— The redshift evolution of the CR input power $\eta\mathcal{E}\mathcal{R}(z)$ for SNe (blue solid), HNe (green solid) and Pop-III HNe (red solid), assuming $\eta = 0.1$. Dashed lines are the total power $\epsilon_p Q_{\epsilon_p}$.

Figure 8 shows the CR input power $\epsilon_p Q_{\epsilon_p}$ versus redshift for this fit, the Pop-III being subdominant (red solid line). However, with a higher density $\bar{n}$, an $f_{pp} = 1$ (at the low energy end) is obtained for Pop-III, while $f_{pp} \sim 0.3$ for SBGs and $f_{pp} \sim 0.03$ for SFGs, which compensates for the lower star formation rates of POP-III stars. (Note that the assumed energy injection might be optimistic because of the uncertainty in f_{pp} and $\xi_{\rm SBG}$.)

4. DISCUSSION AND CONCLUSIONS

In this work we have considered the possible contribution of standard core collapse supernovae and hypernovae to the observed IceCube diffuse neutrino background, including two aspects which, to our knowledge, have not been previously considered in the literature. One of these aspects is the time history of the SNR evolution, which affects the effective total cosmic ray spectral output. Considering the contribution of SNRs and HNRs in the redshift range $z \leq 4$ only, and considering a CR spectral injection power law slope $p = 2$ and a CR injection efficiency which during the Sedov-Taylor phase tapers off as a time power law $\propto t^\alpha$ with $\alpha \leq 0$, we performed de-

tailed calculations of the resulting diffuse neutrino flux and the diffuse gamma-ray flux contributed by SNRs of both the above types. It remains difficult to account for the neutrino data point at 30 TeV as well as for the rest of the higher energy points with any single power law injection spectrum, as pointed out by several authors (Murase et al. 2016; Bechtol et al. 2015; Kistler 2015). However, if we do not include the 30 TeV data point, e.g. by implicitly assuming that it is an extra component, perhaps due to hidden sources (Murase et al. 2016), we find that the neutrino flux contributed by SNe and HNe in SFGs at $z \leq 4$ can explain about 50% of the remaining IceCube observations, without violating the fraction of 14% of the diffuse gamma-ray flux which, according to the Fermi-LAT collaboration, cannot be attributed to unresolved AGNs of known types (Ackermann et al. 2012; Fermi Collaboration 2016).

In view of the observations showing that core-collapse GRBs are associated with SN/HN type Ib/c (e.g. Gehrels et al. 2009), it is pertinent to inquire what may be the potential contribution of such GRBs to the diffuse neutrino and gamma-ray backgrounds discussed here. Although so far there only about seven such associations verified through their spectrum, and a few tens verified through light curves (e.g. Cano et al. 2016), which is a small fraction of all GRBs ($\ll 10\%$), the association is believed to apply to all long GRBs. Note that the SNe associated with GRBs are mostly hypernovae, and all are of type Ib/c, while here in our work the SNe and HNe considered are of all the core collapse types II+Ib/c. At low redshifts, HNe are a fraction $5\%-10\%$ of all core collapse SNe, and only a fraction of order $5\%-10\%$ appears associated with GRBs (Modjaz et al. 2015; Arcavi et al. 2010; Soderberg et al. 2010). Since the average GRB jet beaming correction is roughly 1/100 (Guetta et al. 2005), the fraction of detected GRBs which could be positionally associated with the neutrinos or gamma-rays discussed here is $\lesssim (1/10)(1/10)(1/100) \sim 10^{-4}$, which is negligible in our scenario.

Since at best only a fraction of the IceCube neutrinos can be explained by SNe and HNe in the redshift range $z \leq 4$, the other new aspect considered here is the possible contribution of Pop-III HNe at $4 \leq z \leq 10$. Murase et al. (2016) discussed a possible contribution of very-high-redshift injections. Chang et al. (2016) recently argued that the IceCube generic neutrino sources may reside at high redshifts, but their focus is not on Pop-III remnants. In our case we specifically considered Pop-III HNRs as main sources for both the low and high redshift neutrinos and gamma-rays, and we have used a specific model of the EBL evolution in the Pop-III redshift range (Inoue et al. 2013). The Pop-III SNRs are expected to be more energetic than their lower redshift counterparts, and could contribute significantly to the total CR output. The neutrinos will reach the observer unimpeded, but the gamma-rays produced at high redshifts need to travel longer and have a greater chance to be attenuated by interacting with the EBL.

We find that, aside from the 30 TeV data point, a neutrino flux compatible with IceCube could be obtained by considering a substantial contribution from a Pop-III component, which does not violate the residual diffuse gamma-ray background constraint. Figure 7 is an example of such a fit, where the fiducial parameters $\mathcal{E}_{\rm POP-III} = 10^{52.5}$ erg and $\eta = 0.1$ are used for Pop-III HNRs, which here contribute $\sim 10\%$ of the total neutrino flux. A larger neutrino contribution which still respects the Fermi bounds, as shown in Fig.5, would require $\mathcal{E}_{\rm POP-III} \sim$ a few $\times\, 10^{53}$ erg for the Pop-III rate model of Inoue et al. (2013), or larger for more pessimistic rate models such those of Trenti & Stiavelli (2009); Wise et al. (2012). Thus we conclude that it will be difficult for Pop-III HNRs to dominantly contribute to the observed high-energy backgrounds unless the explosion energy is $\mathcal{E}_{\rm Pop-III} \gtrsim 10^{53}$ erg. On the other hand, the explosion energy for supermassive stars at very-high-redshifts could be larger than $\sim 10^{55}$ erg (Matsumoto et al. 2015). Note that the relative ratio of the neutrino fluxes contributed by the high and low redshift components are largely uncertain. If the fraction of Pop-III HNRs were even higher than assumed here, there would be even less arriving high-energy gamma-rays, further weakening the tension with Fermi-LAT.

We thank Nick Senno for discussions, and we acknowledge support by the National Basic Research Program of China (973 Program grant 2014CB845800 and the National Natural Science Foundation of China grant 11573014 (D.X. and D.Z.G.), by the program for studying abroad supported by China Scholarship Council (D.X.), by Pennsylvania State University (K.M.) and by NASA NNX13AH50G (P.M.).

REFERENCES

Aartsen, M. G., IceCube Collaboration, 2013, Phys. Rev. Lett., 111, 1103
Aartsen, M. G., IceCube Collaboration, 2013, Science, 342, 6161
Aartsen, M. G., IceCube Collaboration, 2015, ApJ, 809, 98
Abel, T., Bryan, G. L., & Norman, M. L., 2002, Science, 295, 93
Ackermann, M., et al. 2012, ApJ, 755, 164
Ackermann, M., et al. 2015, ApJ, 799, 86
Ahlers, M., & Murase, K. 2014, Phys. Rev. D, 90, 023010
Alvarez-Muñiz, J., & Mészáros, P., 2004, Phys. Rev. D, 70, 123001
Anchordoqui, L. A., Hooper,D., Sarlar, S., & Taylor, A. M., 2008, Aph, 29, 1
Anchordoqui, L. A., Paul, T. C., da Silva, L. H. M., Torres, D. F., & Vlcek, B. J., 2014, Phys. Rev. D, 89, 127304
Ando, S., Tamborra, I., & Zandanel, F., 2015, Phys. Rev. Lett., 115, 1101
Arcavi, I. et al., 2010, ApJ, 721, 777
Bechtol, K., Ahlers, M., Di Mauro, M., Ajello, M., & Vandenbroucke, J., 2015, arXiv:1511.00688v1.
Beck, R., 2016, ARA&A, 24, 4
Beresnyak, A., Jones, T. W., & Lazarian, A., 2009, ApJ, 707, 1541
Berezhko, E. G., 2014, NuPhS, 256, 23
Berezinskii, V. S., & Smirnov, A. I., 1975, Ap&SS, 32, 461
Berezinsky, V., & Blasi, P., 2012, Phys. Rev. D, 85, 123003
Bromm, V., & Loeb, A., 2006, ApJ, 642, 382
Bustamante, M., Baerwald, P., Murase, K., & Winter, W., 2015, Nature Communications, 6, 6783
Cano, Z., Wang, S. Q., Dai, Z. G., & Wu, X. F., 2016, arXiv:1604.03549
Caprioli,D., Pop, A. R., & Spitkovsky, A., 2015, ApJ, 798, 28
Chang, X. C., & Wang, X. Y., 2014, ApJ, 793, 131
Chang, X. C., & Wang, X. Y., 2015, ApJ, 805, 95
Chang, X. C., Liu, R. Y., & Wang, X. Y., 2016, arXiv:1602.06625v1.
Chen, Ke-Jung, 2014, Int. J. Mod. Phys. D, 23, 30008
Chevalier, R. A., & Claes, F., 2001, ApJ, 558, L27
Crocker, R. M., 2012, MNRAS, 423, 3512
Dai, Z. G., & Lu, T., 2002, 580, 1013
Dai, Z. G., Zhang, B., Gou, L. J., Mészáros, P., & Waxman, E., 2002, ApJ, 580, L7
Dermer, C. D., 2002, arXiv:astro-ph/0202254
Dermer, C. D., Murase, K., & Inoue, Y., 2014, ApJ, 793, 131
de Souza, R. S., Yoshida, N., & Ioka, K., 2011, A&A, 533, 32
Fermi-LAT Collaboration, 2016, arXiv:1601.04323.
Draine, B. T., & Woods, D. T., 1991, ApJ, 383, 621
Drury, L. O'c., 2011, MNRAS, 415, 1807
Fang, K., Kotera, K., Murase, K., & Olinto, A. V., 2014, Phys. Rev. D, 90, 103005
Finke, J. D., Razzaque, S., & Dermer, C. D., 2010, ApJ, 712, 238
Fox, O. D., et al., 2011, ApJ, 741, 7
Fox, D. B., Kashiyama, K., & Mészáros, P., 2013, ApJ, 774, 74
Gaisser, T. K., 1990, Cosmic rays and particle physics (Cambridge University Press),
Gao, S., Toma, K., & Mészáros, P., 2011, Phys. Rev. D, 83, 3004
Gehrels, N., Ramirez-Ruiz, E., & Fox, D. B., 2009, ARA&A, 47, 567
González-Casanova, D. F., De Colle, F., Ramirez-Ruiz, E., & Lopez, L. A., 2014, ApJ, 781, 26
Gou, L.J., Fox, D.B. & Mészáros, P., 2007, ApJ, 668, 1083
Guetta, D., Piran, T., & Waxman, E., 2005, ApJ, 619, 412
Guetta, D., & Della Valle, M., 2007, ApJ, 657, L73
Gupta, D., & Zhang, B., 2007
He, H. N., Wang, T., Fan, Y. Z., Liu, S. M., & Wei, D. M., 2013, Phys. Rev. D, 87, 063011
Hopkins, A. M., & Beacom, J. F., 2006, ApJ, 651, 142
Hosokawa, T., Omukai, K., Yoshida, N., & Yorke, H. W., 2011, Science, 334, 1250
Inoue, Y., Inoue, S., Kobayashi, M., Makiya, R., Niino Y., & Totani, T., 2013, ApJ, 768, 1971
Iocco, F., Murase, K., Nagataki, S., & Serpico, P. D., 2008, ApJ, 675, 937
Ioka, K., & Mészáros, P., 2010, ApJ, 709, 1337
Iwamoto, K., et al., 1998, Nature, 395, 672
Iwamoto, N., Umeda, H., Tominaga, N., Nomoto, K., & Maeda, K., 2005, Science, 309, 4511
Keeney, B. A., Danforth, C. W., Stocke, J. T., et al., 2006, ApJ, 646, 951
Keshet, U., Waxman, E., & Loeb, A., 2004, ApJ, 617, 281
Kistler, M. D., 2015, arXiv:1511.01530v1.
Koo, B. C., Moon, D. S., Lee, H. G., Lee, J. J., & Matthews, K., 2007, ApJ, 657, 308
Kosenko, D., Ferrand, G., & Decourchelle, A., 2014, MNRAS, 443, 1390
Lacki, B. C., & Thompson, T. A., 2013, ApJ, 762, 29
Lacki, B. C., Horiuchi, S., & Beacom, J. F., 2014, ApJ, 786, 40
Liu, R. Y., Wang, X. Y., Inoue, S., Crocker, R., & Aharonian, F., 2014, Phys. Rev. D, 89, 3004
Loeb, A., & Waxman, E., 2006, Jour. Cosmology and Astro-Particle Phys. , 5, 3
Lopez, L. A., Ramirez-Ruiz, E., Castro, D., & Pearson, S., 2013, ApJ, 764, 50
Matsumoto, T., Nakauchi, D., Ioka, K., Heger, A, & Nakamura, T., 2015, ApJ, 810, 64
Mazzali, P. A., et al., 2003, ApJ, 599, L95
Mészáros, P., 2014, NuPhS, 256, 241
Mészáros, P., & Waxman, E., 2001, Phys. Rev. Lett., 87, 171102
Modjaz, M., Liu, Y. Q., Bianco, F. B., & Graur, O., 2015, arXiv:1509.07124
Murase, K., 2008, Phys. Rev. D, 78, 101302(R)
Murase, K., 2015, AIPC, 1666, 0006
Murase, K., Ahlers, M., & Lacki, B. C., 2013, Phys. Rev. D, 88, 121301(R)
Murase, K., Beacom, J. F., & Takami, H., 2012, Jour. Cosmology and Astro-Particle Phys. , 08, 030
Murase, K., Guetta, D., & Ahlers, M., 2016, Phys. Rev. Lett., 116, 071101
Murase, K., Inoue, S., & Nagataki, S., 2008, ApJ, 689, L105
Murase, K., Inoue, Y., & Dermer, C. D., 2014, Phys. Rev. D, 90, 023007
Murase, K., & Ioka, K., 2013, Phys. Rev. Lett., 111, 121102
Murase, K., Ioka, K., Nagataki, S., & Nakamura, T., 2006, ApJ, 651, L5
Murase, K., Mészáros, P., & Zhang. B., 2009, Phys. Rev. D, 79, 103001
Neronov, A., & Semikoz, D., 2016, Aph, 75, 60
Ohira, Y., Murase, K., & Yamazaki, R., 2011, A&A, 513, 17
Petropoulou, M., Dimitrakoudis, S., Padovani, P., Mastichiadis, A., & Resconi, E., 2015, MNRAS, 448, 2412
Planck Collaboration, 2015, arXiv:1502.01589v2.
Ramirez-Ruiz, E., & MacFadyen, A. I., 2010, ApJ, 716, 1028
Rees, M. J., & Ostriker, J. P., 1977, ApJ, 179, 541
Robishaw, T., Quataert, E., & Heiles, C., 2008, ApJ, 680, 981
Salamon, M. H., & Stecker F. W., 1998, ApJ, 493, 547
Salvesen, G., Raymond, J. C., & Edgar, R., 2009, ApJ, 702,327
Schneider, R., Guetta, D., & Ferrara, A., 2002, MNRAS, 334, 173
Sedov, L. I., 1959, Similarity and Dimensional Methods in Mechanics (New York: Academic)
Senno, N., Mészáros, P., Murase, K., Baerwald, P., &Rees, M. J., 2015, ApJ, 806, 24
Senno, N., Murase, K., & Mészáros, P., 2016, Phys. Rev. D, 93, 083003
Silk, J., 1977, ApJ, 211, 638
Soderberg, A. M., et al., 2010, Nature, 463, 513
Stecker, F. W., Done, C., Salamon, M. H., & Sommers, P., 1991, Phys. Rev. Lett., 66, 2697
Stecker, F. W., 2013, Phys. Rev. D, 88, 047301
Strickland, D. K., & Heckman, T. M., 2009, ApJ, 697, 2030
Sutherland, Ralph S., & Dopita, M. A., 1993, ApJS, 88, 253
Sveshnikova, L. G., 2003, A&A, 409, 799
Tamborra, I., Ando, S., & Murase, K., 2014, Jour. Cosmology and Astro-Particle Phys. , 9, 43
Tamborra, I., & Ando, S., 2016, Phys. Rev. D, 93, 053010
Thompson, T. A., Quataert, E., Waxman, E., Murray, N., & Martin, C. L., 2006, ApJ, 645, 186
Taylor, G., 1950, RSPSA, 201, 159
Taylor, A. M., Gabici, S., & Aharonian, F., 2014, Phys. Rev. D, 89, 101003
Taylor, M., et al. 2014, ApJ, 792, 135
Toma, K., Yoon, S. C., & Bromm, V., 2016, Space Science Reviews

Tominaga, N., Iwamoto, N., & Nomoto, K., 2014, AIP Conference Proceedings, 1594, 52
Trenti, M., & Stiavelli, M., 2009, ApJ, 694, 879
Umeda, H., & Nomoto, K., 2003, Nature, 422, 871
Wang, X. Y., Razzaque, S., Mészáros, P., & Dai, Z. G., 2007, Phys. Rev. D, 76, 3009
Wang, X. Y., & Dai, Z. G. 2009, ApJ, 691, 67
Waxman, E., & Bahcall, J. 1997, Phys. Rev. Lett., 78, 2292
Whalen, D. J., Joggerst, C. C., Fryer, C. L., Stiavelli, M., Heger, A., & Holz, D. E., 2013, ApJ, 168, 95
Wise, J. H., & Abel, T., 2005, ApJ, 629, 615
Wise, J. H., Turk, M. J., Norman, M. L., & Abel, T., 2012, ApJ, 745, 50
Xiao, D., & Dai, Z. G. 2014, ApJ, 790, 59
Xiao, D., & Dai, Z. G. 2015, ApJ, 805, 137
Yang, Y. P., Wang, F. Y., & Dai, Z. G., 2015, A&A, 582, 7
Yüksel, H., Kistler, M. D., Beacom, J. F., & Hopkins, A. M., 2008, ApJ, 683, L5